特別掲載

Performance of Various X-ray Film/screen Systems in Demonstrating Small Simulated Low-density Lung Nodules

Yuichiro Maruyama

Department of Radiology, Shinshu University School of Medicine

X線フィルム/スクリーンシステムの物理特性の違いによる肺野低濃度結節影の検出能の検討

丸山雄一郎

肺野の早期肺癌などの淡く小さい結節影を検出するために，胸部単純X線像の肋骨や縦隔等に重なる低濃度肺野域において，肺野内の結節影の検出能にX線フィルム/スクリーンのコントラストや鮮鋭度，粒状性などが与える影響について検討した．胸部単純撮影用X線フィルム/増感紙システムには以下の6種類(富士メディカル製：HR3，super/HR3，super/HR4，super30/HR3，UR-1，UR-2)を用いた．高さ10mmと5mmで球形，上1/2および上1/3が球形で末広がりの3種類の疑似結節(塩化ビニール製)を撮影し，結節周囲領域の黒化度が0.27，0.33，0.4および0.5のフィルムを各20枚，濃度条件は同じであるが結節を置かずに撮影したものを40枚作製し，合計3840枚について放射線診断医8名が疑似結節の見え方を5段階の確診度で判定した．判定結果をROC解析しAz値を計算してpaired-t検定を行った．辺縁が明瞭な結節影の検出率は高く($P < 0.05$)，輪郭の明瞭さが検出能に影響を与えていた．低濃度域で結節の検出率は低下したが，低濃度域で高コントラストを有する感光システムは良好な検出率を示した($P < 0.05$)．X線フィルムの特性曲線において低濃度領域でコントラストが高いことが望ましい．また低濃度領域で辺縁の不鮮明な結節影の検出率を高めるためにはシステムの粒状性も重要である．高コントラストで粒状性にも優れた胸部撮影システムを使用することが，肺野の低濃度領域に存在する結節影の検出に適する．

Research Code No. : *208*

Key words : *Radiography, Film screen system Observer performance, Lung nodule*

Received Dec. 10, 1997; revision accepted Jun. 18, 1998
信州大学医学部放射線医学教室

Introduction

A high-quality, conventional chest radiograph should be obtained in lung cancer screening programs to efficiently detect the faint, small nodular shadows due to early lung cancer in the lung fields, although it is difficult to image the entire lung field within the linear part of the characteristic curve of the screen-film system owing to the wide variation in tissue density in the thorax, which ranges from the well aerated lung superimposed on the intercostal spaces to the lung area superimposed on the heart or diaphragm[1]. In the detection of early cancer in the lung fields, it is important to consider the very low density (CT values of nearly -600 HU to -300 HU) commonly exhibited by early adenocarcinomas in the lung. The detectability of such nodules would be greatly influenced by the contrast and noise characteristics of the photographic system, the complexity of anatomical structures around the nodule, the characteristics of the observation system for x-ray films, the interpreter, and so on[2)-9)]. The choice of x-ray film/screen system basically determines the efficacy of screening; specifically, the contrast characteristics of x-ray films together with noise level, which varies at different optical densities, affect the detectability of nodular shadows[10)-14)]. The present study was carried out to determine the most suitable sensitometric characteristics and to assess the effects of the noise level of the x-ray film/screen system on the detectability of nodular shadows within the lung fields, particularly in low-density areas.

Materials and Methods

1. Materials

The x-ray equipment and screen/film combinations used in the study are listed below.

X-ray system: HD150B-30 (Shimadzu Corporation, Tokyo), X-ray tube: P38C (focal spot size, 0.3/0.8 mm)

X-ray film/ screen systems: six combinations, including HR-S/HR-3 (HR 3), SUPER HR-S/HR-3 (super/HR-3), SUPER HR-

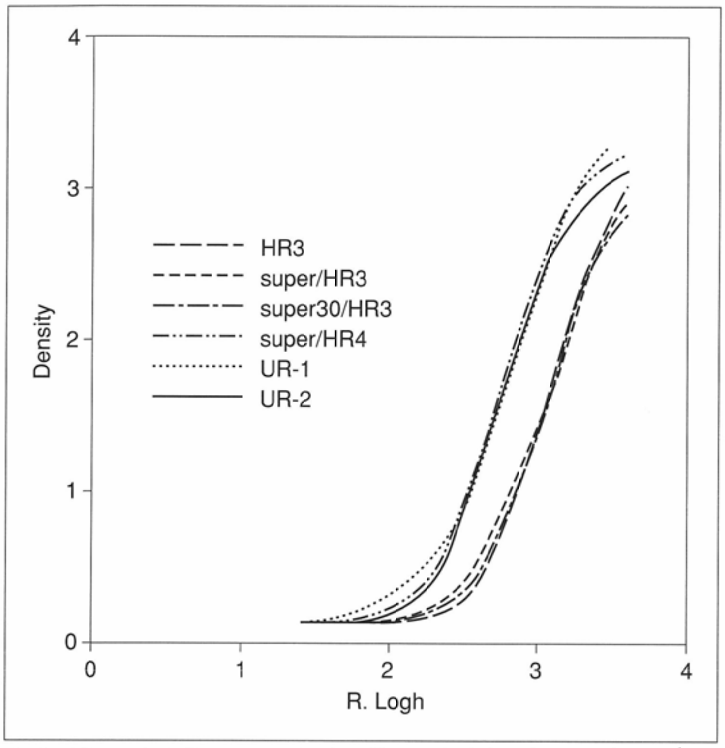

Fig.1 Characteristic curves plotting film optical density as a function of log relative exposure

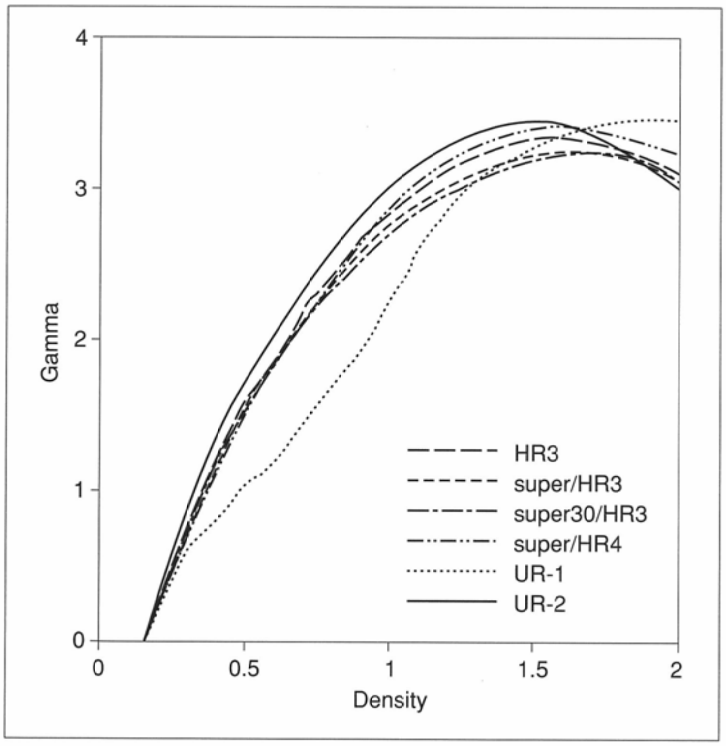

Fig.2 Density-gamma curves of the six film/screen systems

S30/HR-3 (super30/HR-3), SUPER HR-S/HR-4 (super/HR-4), UR-1/HG-M (UR-1), and UR-2/HG-M (UR-2) (Fuji Medical Systems, Tokyo).

Of these, UR-1 and UR-2 have been commercially available since 1993. Both of these are superior to the older HR series (HR-3, super/HR-3, super/HR-4, and super30/HR-3) with respect to noise.

Processing of radiographs: processor, KX-500 automatic film processor (Konica Corporation, Tokyo); developer, RD-3; development temperature, 32.5°C. The characteristic curves under the above conditions and the density gamma curves are shown in Figs.1 and 2, and root mean square (RMS) values are shown in Fig.3. The characteristic curves, the density gamma curves and RMS values were counted using our sample films. The characteristics of each system are shown in Table 1.

2. Simulated nodules

Six types of simulated nodules were prepared from vinyl chloride in two sizes (5 and 10 mm) and three shapes (spherical, 1/2 flared spherical, and 2/3 flared spherical). The base diameters of the 1/2 and 2/3 flared spherical nodules were identical: 7.5 mm for the 5-mm size and 15 mm for the 10-mm size (Fig.4). The spherical nodules represented well-defined nodules, and the flared spherical nodules represented poorly defined nodules (Fig.5).

3. X-ray films for interpretation

Imaging parameters: x-ray tube voltage, 120 kVp; tube current, 100 mA; FFD, 200 cm.

Exposure time: Four exposure times were selected to obtain background optical density (BOD) values for the nodules of 0.27, 0.33, 0.4, and 0.5 for the nodules of 5 mm and 10 mm size. Twenty radiographs were printed on an x-ray film (14" by 14") on which a 4 by 4 square grid (with each frame 6 cm by 6 cm in size) had been predetermined with a simulated nodule placed in it. X-ray exposure was performed with a flat acrylic plate with a thickness of 20 cm placed on the film to adjust the radiographic density.

X-ray films for interpretation were prepared by dividing the x-ray films obtained as described above into separate frames of 2880 grids with all types of simulated nodules generated for interpretation (20 grids for each combination of imaging parameters: 6 screen/film systems, 6 nodule types, and 4 different density conditions). In addition, 960 grids without nodules were generated (40 grids for each combination of imaging parameters: 6 photographic systems and 4 density conditions). A total of 3840 grids were randomly arranged and placed on a view box with a brightness of approximately 6000 lux. During interpretation, areas surrounding the grids were covered to make them dark.

4. Interpretation

Eight diagnostic radiologists with 2 to 33 years of clinical experience evaluated all test grids. Prior to the interpretation of x-ray films, a sample film in which the six types of simulated

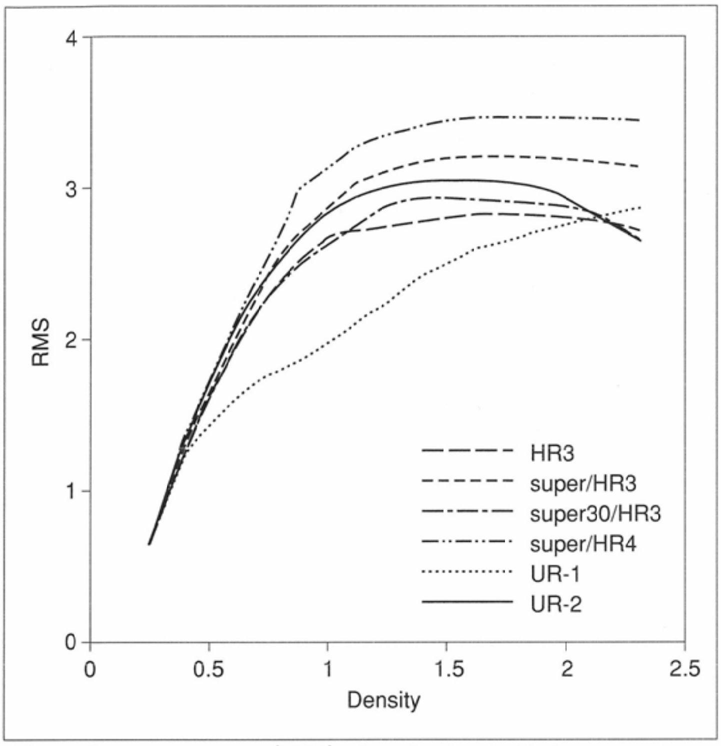

Fig.3 Root mean square (RMS) values for the six film/screen systems

Table 1 Characteristics of the six film/screen systems

Film/screen system	Contrast type	Subjective evaluation of noisiness
HR-3	standard	good
super/HR-3	standard	degraded (slight)
super30/HR-3	standard	degraded (slight)
super/HR-4	standard	most degraded
UR-1	standard	excellent
UR-2	high (slight)	excellent

HR-3 = HR-S/HR-3, *super/HR-3* = SUPER HR-S/HR-3, *super/HR-4* = SUPER HR-S/HR-4, *super30/HR-3* = SUPER HR-S30/HR-3, *UR-1* = UR-1/HG-M, *UR-2* = UR-2/HG-M

nodules had been imaged at BOD 0.5 were shown to the interpreters. They then evaluated all test grids in random sequence and recorded the presence or absence of nodule on each grid. The following five levels of confidence were used: (1) nodular shadow absent, (2) nodular shadow probably absent, (3) nodular shadow possibly absent or present, (4) nodular shadow probably present, (5) nodular shadow present. The time required for evaluation of each film was approximately 5 seconds, and images were observed at a viewing distance of 40 to 50 cm. However, these conditions could be adjusted as desired by the interpreter.

5. Statistical analysis

The accuracy values for 144 combinations of the test parameters (consisting of 6 nodule types, 4 optical densities and 6 screen/film systems) were calculated for each of the eight interpreters. Moreover, receiver operating characteristic (ROC) analysis[15),16)] was performed by generating ROC curves using the ROCFIT program to calculate the area under the curve (Az). Mean values of 8 observers between the groups were compared using Student's t-test or Welch's t-test. The statistical software package used was SPSS™.

Results

1. Detection rate of simulated nodules according to the photographic system

Table 2 shows the results of the interpretation experiment. For 10-mm nodules, Az was high for all photographic systems examined. Only at BOD 0.27, was UR-2 superior to other systems, particularly as compared with HR-4 or HR-3.

For 5-mm nodules, UR-2 gave the best results, followed by the HR series. UR-1 was inferior to the others; in particular, the difference was large at BOD 0.27, becoming less as optical density increased. When BOD was 0.40, no statistically significant difference was recognized among systems, excluding UR-1, and at BOD 0.50 the results were identical. In a comparison between

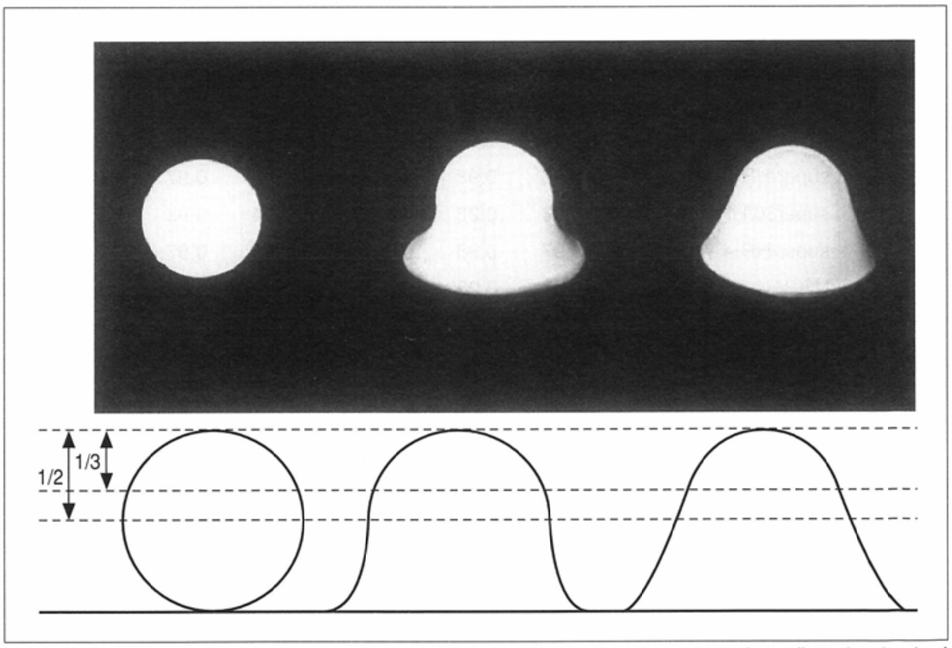

Fig.4 Photographs and dimensions of spherical, 1/2 flared spherical, and 2/3 flared spherical simulated nodules

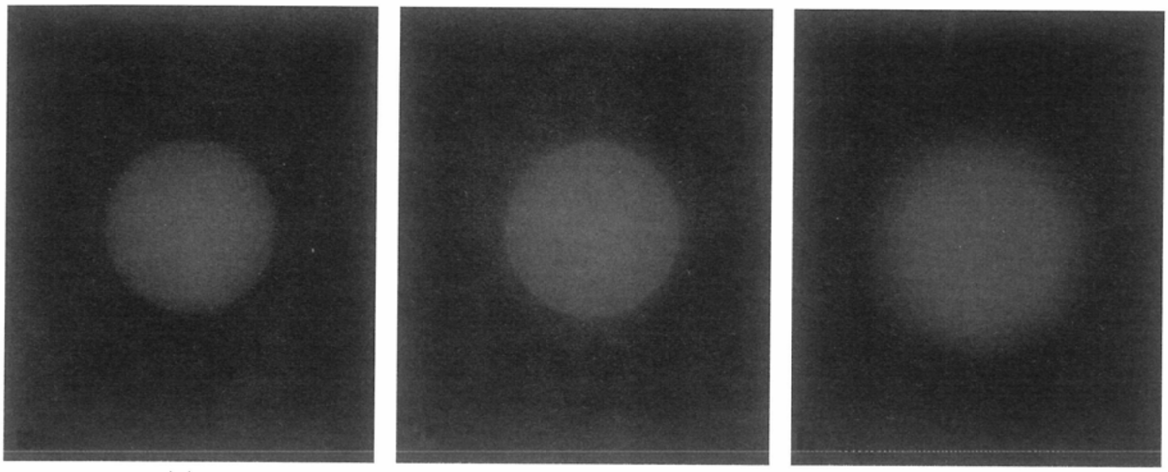

(A) (B) (C)

Fig.5 End-on images of the simulated nodules shown on a conventional radiograph: (A) spherical, (B) 1/2 flared spherical, and (C) 2/3 flared spherical

super/HR-3 and super/HR-4, in which the same x-ray film and different screens were used, the latter was inferior at BOD 0.27.

2. Detection rate of nodules according to film density

For 10-mm nodules, UR-2 was the best in detecting nodules at BOD 0.27, as shown in Table 2. At BOD values of 0.33, 0.40, and 0.50, detectability was higher than at BOD 0.27, and there was no statistically significant difference between 0.33, 0.40 and 0.50. For 5-mm nodules, UR-2 showed the best detectability at a density of 0.27, followed by the HR series and UR-1. Fig.6 shows the ROC curves for each imaging system shown with 2/3 spherical nodules. No differences were detected between UR-2 and the HR series at BOD 0.33 or higher. The detectability of UR-1 was frequently lower than that of UR-2 and the HR series. Figs.7A, and 7B illustrate averaged ROC curves. In the HR series and UR-1, detectability was markedly decreased at BOD 0.27, compared with density values of 0.33 to 0.50 ($P < 0.01$). For UR-2, on the other hand, almost identical detectability was obtained, compared with the results obtained at density values of 0.27 to 0.50.

3. Detection rate of nodules according to their configuration

Table 3 shows differences in detectability according to the shape of the nodule for 1/2 and 2/3 flared spherical nodules with identical base diameters. For 10-mm nodules, Az values were larger for 1/2 flared spherical nodules than for 2/3 flared spherical nodules, irrespective of the system used, when BOD was 0.27. In particular, statistically significant differences were recognized ($P < 0.01$) for super/HR-3, super/HR 4, and UR-2. Even for 5-mm nodules, the Az values of 1/2 flared spherical nodules were

Table 2 Observer performance for the six film/screen systems indicated by the area under the ROC curve (Az)

Thickness	Film/screen system	Shape											
		Spherical				1/2 flared spherical				2/3 flared spherical			
10mm	Density	0.27	0.33	0.40	0.50	0.27	0.33	0.40	0.50	0.27	0.33	0.40	0.50
	HR-3	0.92	0.97	0.98	0.98	0.94	0.97	0.98	0.98	0.85	0.96	0.98	0.98
	super/HR-3	0.91	0.97	0.98	0.98	0.92	0.97	0.98	0.98	0.80	0.94	0.98	0.98
	super30/HR-3	0.95	0.98	0.98	0.98	0.94	0.98	0.98	0.98	0.90	0.96	0.98	0.98
	super/HR-4	0.92	0.97	0.98	0.98	0.93	0.97	0.98	0.98	0.78	0.92	0.98	0.98
	UR-1	0.92	0.97	0.98	0.98	0.89	0.97	0.98	0.98	0.86	0.96	0.98	0.98
	UR-2	0.97	0.97	0.98	0.98	0.97	0.97	0.98	0.98	0.93	0.97	0.98	0.98
5mm	Density	0.27	0.33	0.40	0.50	0.27	0.33	0.40	0.50	0.27	0.33	0.40	0.50
	HR-3	0.79	0.93	0.97	0.98	0.79	0.93	0.97	0.98	0.77	0.89	0.95	0.98
	super/HR-3	0.72	0.86	0.97	0.97	0.80	0.88	0.94	0.97	0.69	0.89	0.97	0.96
	super30/HR-3	0.81	0.93	0.96	0.97	0.73	0.88	0.97	0.97	0.68	0.90	0.96	0.97
	super/HR-4	0.60	0.91	0.96	0.98	0.63	0.94	0.96	0.98	0.68	0.92	0.96	0.98
	UR-1	0.69	0.88	0.88	0.96	0.75	0.90	0.95	0.96	0.67	0.87	0.92	0.96
	UR-2	0.88	0.95	0.96	0.98	0.89	0.96	0.97	0.98	0.85	0.93	0.97	0.97

* statistically significant difference ($P < 0.05$)

HR-3 = HR-S/HR-3, *super/HR-3* = SUPER HR-S/HR-3, *super/HR-4* = SUPER HR-S/HR-4, *super30/HR-3* = SUPER HR-S30/HR-3, *UR-1* = UR-1/HG-M, *UR-2* = UR-2/HG-M

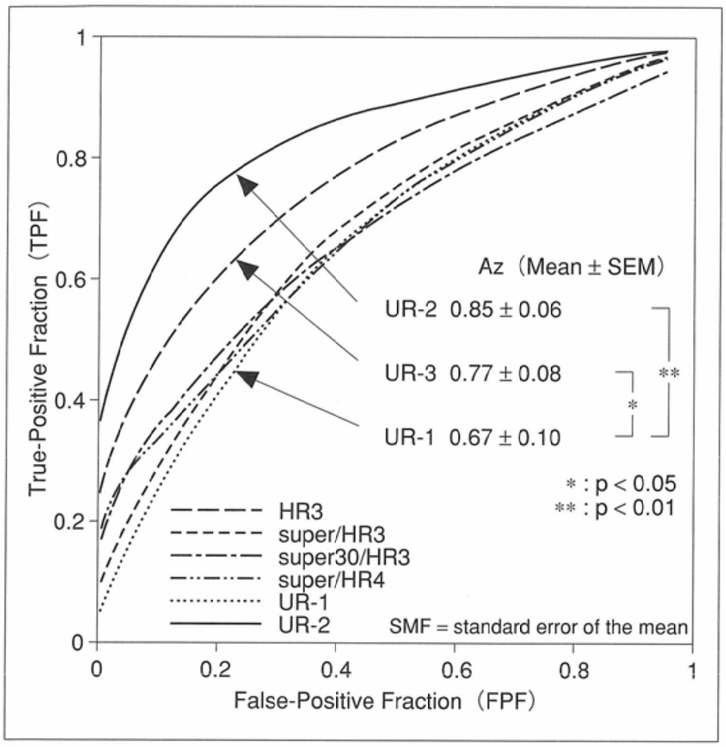

Fig.6 ROC curves for the six film/screen systems (5-mm, 2/3 flared spherical nodule at 0.27 density)

generally higher. In low-density areas using super/HR-3 and UR-1, in particular, the differences were the largest. However, no statistically significant differences were recognized.

Analysis of the results shown in Tables 1 and 2, in a comparison of spherical and 2/3 flared spherical nodules, revealed statistically significant differences ($P < 0.05$) between super/HR 3, super/HR-4, and UR-2 for 10-mm nodules when BOD was 0.27. In a comparison of spherical and 1/2 flared spherical nodules, no statistically significant differences were recognized between systems, irrespective of the optical density.

Discussion

In frontal chest radiographs, approximately 43% of the lung area and approximately 26% of the lung volume may be obscured by cardiac, mediastinal, and subdiaphragmatic structures[1]. It is important to achieve high sensitivity to clearly visualize the areas that tend to be obscured. Several methods have been employed to overcome this difficulty, including appropriate selection of the screen/film system and the use of high tube kV settings, compensation filters, and so forth. Several kinds of wide-latitude film for thoracic imaging are now available: wide-latitude film minimizes film darkening in high-exposure areas, and extended-latitude film further provides greater darkening in low-exposure areas, which might lead us to expect a higher contrast in visualizing any abnormality in these regions. However, contrary to this expectation, some extended-latitude films may not improve the recognition of low-density nodules in underexposed areas owing to their low gradient in the low-density range of the characteristic curve.

To clarify these points, more detailed investigations into the effect of the characteristic curve are warranted. In the present

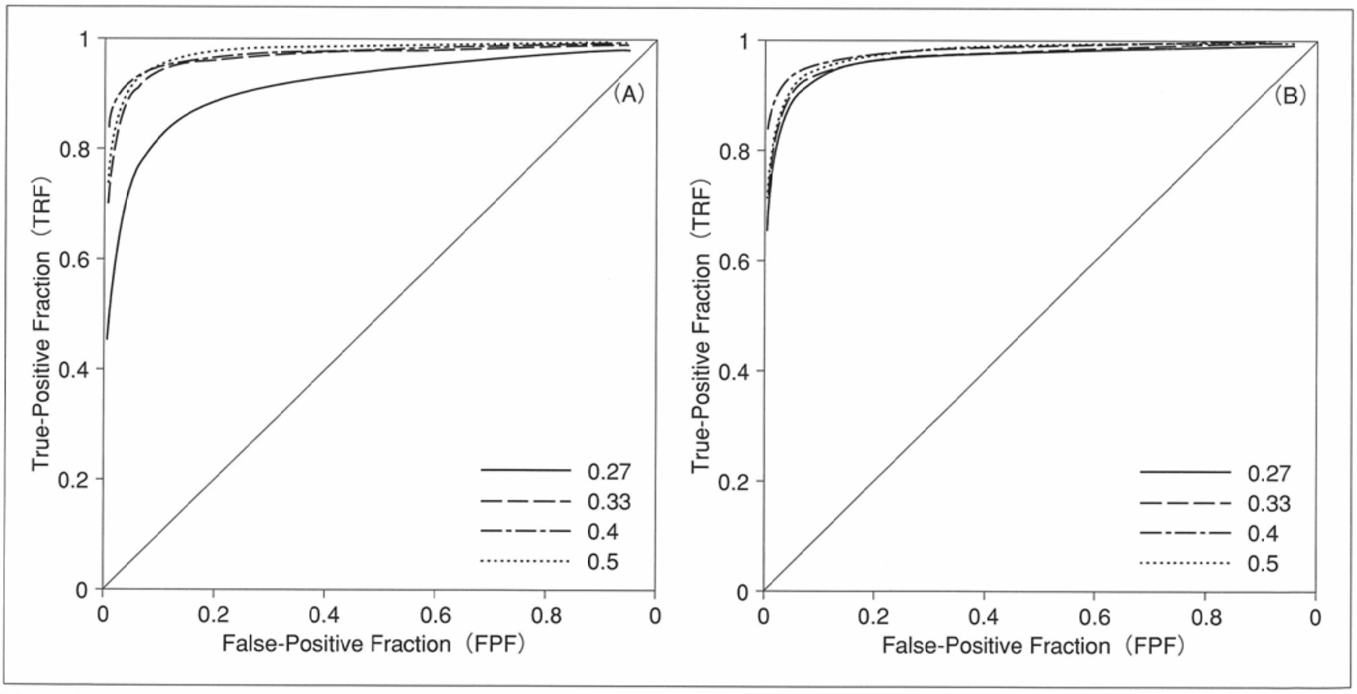

Fig.7 Averaged ROC curves for eight observers in detecting simulated nodules: (A) UR-1/HG-M, (B) UR-2/HG-M

Table 3 Observer performance evaluated by the area under the ROC curve (Az)

		10mm thickness			5mm thickness		
		2/3 flared spherical Az		1/2 flared spherical Az	2/3 flared spherical Az		1/2 flared spherical Az
HR-3	0.27	0.85		0.94	0.77		0.79
	0.33	0.96		0.97	0.89		0.93
	0.4	0.98		0.98	0.95	<	0.97
	0.5	0.98		0.98	0.98		0.98
super/HR-3	0.27	0.80	<<	0.92	0.69		0.80
	0.33	0.94		0.97	0.89		0.88
	0.4	0.98		0.98	0.97	>	0.94
	0.5	0.98		0.98	0.96		0.97
super30/HR-3	0.27	0.90		0.94	0.68		0.73
	0.33	0.96		0.98	0.90		0.88
	0.4	0.98		0.98	0.96		0.97
	0.5	0.98		0.98	0.97		0.97
super/HR-4	0.27	0.78	<<	0.93	0.68		0.63
	0.33	0.92	<	0.97	0.92		0.94
	0.4	0.98		0.98	0.96		0.96
	0.5	0.98		0.99	0.98		0.98
UR-1	0.27	0.86		0.89	0.67		0.75
	0.33	0.96		0.97	0.87		0.90
	0.4	0.98		0.98	0.92		0.95
	0.5	0.97	<	0.98	0.96		0.96
UR-2	0.27	0.93	<<	0.97	0.85		0.89
	0.33	0.97		0.97	0.93		0.96
	0.4	0.98		0.98	0.97		0.97
	0.5	0.98		0.98	0.97		0.98

" < " and " << " mean statistically significant difference (" < " : $P < 0.05$, " << " : $P < 0.01$)

study, six x-ray film/screen systems with various characteristic curves and noise characteristics were used to investigate the relationship between these photographic characteristics of the system and the detection rate of faint nodules in low-density areas. Additional studies were performed to investigate the relationship between the sharpness of the nodule contour and the detection rate. The ability to detect a nodule depends upon a number of factors, including nodule size and density, sharpness of boundaries, noise in the radiograph, surrounding (anatomical) complexity and viewing conditions. Theoretically, Photographic contrast C is defined as follows:

$$C = 0.434 \times G \times d \times (\mu 1 - \mu 2)$$

Where C: contrast of the object, G: gradient of the film at the density level of interest, d: thickness of the nodule, and $\mu 1$ and $\mu 2$: linear attenuation coefficients of the nodule and the surrounding material, respectively. Because the present study focused on the detection of nodules in specific density regions, particularly those with relatively low optical density values of 0.50 or less, corresponding to the lung fields superimposed over the heart, diaphragm, and ribs on chest x-ray films, the value of G was not constant, with lower values in less-exposed regions (Fig.2). Due to the differences in these photographic features of the systems, the detection of nodules was inconsistent among the systems. By using UR-2 with a maximum gradient, the best results were obtained for detecting 10-mm nodules at the lowest density of 0.27. For 10-mm nodules, nodular shadows were detected satisfactorily when the density was high, irrespective of the characteristics of the photographic system. The 5-mm nodules were again detected most satisfactorily using UR-2 at any optical density. UR-1 was inferior, although not significantly different from the HR series. This finding emphasizes the primary importance of film contrast in low-density areas. Next, at a low optical density of 0.27, the noise of the film resulted in low detectability in super/HR-4, which showed the worst value for RMS (Fig.3).

Detectability depends on the sharpness of the nodule's margins[6),17)]. To investigate this factor, 3 types of nodule configuration were used in this study: spherical, 1/2 flared spherical, and 2/3 flared spherical nodules of the same thickness. For 10-mm nodules, detectability was low for 2/3 flared spherical nodules at a low optical density of 0.27, with little difference between spherical and 1/2 flared spherical nodules, which indicates that the sharpness of the margins determines the detectability of the nodule. Detectability was further decreased in the HR-4 system, probably due to the inferior noise characteristics of this system.

No significant difference was observed between spherical and 2/3 flared spherical nodules with a thickness of 5 mm. This was presumably because the detectability of the latter type might be enhanced by the difference in the base area. From these findings, the sharpness of the margins of nodular shadows presumably improves the detectability of the nodule when a system which provides high-contrast images is employed. However, by far the most important factor is contrast. When a low-contrast system is used, the sharpness of the contours might not result in enhanced of detectability.

Based on the findings of the present study, we conclude that diagnosis should be performed using a high-contrast x-ray image with superior noise to characteristics detect nodular lesions in low-density areas where the lung fields are superimposed over the ribs, the mediastinum, or other structures. The results of this study also indicate that photographic systems equivalent to UR-2 which can provide high-contrast images with superior noise characteristics are most suitable for the detection of nodules in low-density areas within the lung fields. Portions of the lung fields superimposed over the ribs, mediastinum, and diaphragm tend to become low-density areas when such a system is used. To overcome this problem, it is desirable to use other methods such as high-voltage imaging, compensating intensifying screens, compensating x-ray filters, and so on.

Conclusion

1. In order to improve the detectability of low-density nodules in areas of low optical density, a photographic system that maintains high contrast in low-density areas should be employed. Therefore, it is desirable that the characteristic curve of the x-ray film selected exhibit high contrast even in low-density areas.
2. In order to improve the detectability of nodular shadows with unsharp margins in low-density areas, the noise characteristics of the system should also be carefully considered.
3. The use of a chest x-ray system with high contrast and improved noise level, such as the UR-2 system, is appropriate for the detection of peripheral early lung cancers in low-density areas within the lung.

Acknowledgements: The author would like to thank Professor Shusuke Sone M.D. for comments during the preparation of this manuscript.

References

1) Chotas H, Ravin C: Chest radiography: Estimated lung volume and projected area obscured by the heart, mediastinum, and diaphragm. Radiology 193: 403-404, 1994
2) Rossmann K: Spatial fluctuations of X-ray quanta and the recording of radiographic mottle. AJR 90: 863-869, 1963
3) Gray J, Taylor K, Hobbs B: Detection accuracy in chest radiography. AJR 131: 247-253, 1978
4) Kundel H: Images, image quality and observer performance new horizons in radiology lecture. Radiology 132: 265-271, 1979
5) Sorenson J, Mitchell C, Armsrong II J et al. Effects of improved contrast on lung-nodule detection: a clinical ROC study. Invest Radiol 22 772-790, 1987
6) Kundel H, Nodine C, Thickman D, et al: Nodule detection with and without a chest image. Invest Radiol 20: 94-99, 1985
7) Kundel H: Peripheral vision, structured noise and film reader error. Radiology 114: 269-273, 1975
8) Li F, Sone S, Kiyono K: Lung nodule conspicuity using unsharp mask filters with storage phosphor-based computed radiography. Acta Radiologica 38: 99-103, 1997
9) Ise T, Abe M, Endou Y et al: Study report on exposure conditons in daily X-ray examinations. Jpn J Radiol Technol 53: 1826-1849, 1997
10) Chakraborty D, Breatnach E, Yester M, et al: Digital and conventional chest imaging: A modified ROC study of observer performance using simulated nodules. Radiology 158: 35-39, 1986
11) Li F, Sone S, Kiyono K, et al: Detectability of simulated nodules on chest phantom by Fuji computed radiography: Comparison of different nodule sizes, configurations and tube voltages. Nippon acta radiologica 57: 104-109, 1997
12) Logan P, Tunney T, McCoy C, et al: Comparison of a new dual characteristic film-screen system (insight) with a standard film-screen system for chest radiology. Br J Radiol 67: 162-165, 1994
13) Schaefer-Prokop CM, Prokop M, Schmidt A et al: Selenium radiography versus storage phosphor and conventional radiography in the detection of simulated chest lesions. Radiology 201: 45-50, 1996
14) Samei E, Flynn M, Eler W: Simulation of subtle lung nodules in projection chest radiography. Radiology 202: 117-124, 1997
15) Metz C: ROC methodology in radiologic imaging. Invest Radiol 21: 720-733. 1986
16) Metz C: Some practical issues of experimental disign and data analysis in radiological ROC studies. Invest Radiol 24: 234-245, 1989
17) Hemmingsson A, Jung B, Lonnerholm T : Perception of simulated lesions in the lung. Acta Radiologica Diagnosis 16: 494-502, 1975